

Deep-ultraviolet light-emitting device realized via a hole-multiplication process

H. Zhu, C. X. Shan, B. H. Li, Z. Z. Zhang, B. Yao et al.

Citation: *Appl. Phys. Lett.* **99**, 101110 (2011); doi: 10.1063/1.3637575

View online: <http://dx.doi.org/10.1063/1.3637575>

View Table of Contents: <http://apl.aip.org/resource/1/APPLAB/v99/i10>

Published by the [American Institute of Physics](#).

Related Articles

Cavity suppression in nitride based superluminescent diodes

J. Appl. Phys. **111**, 083106 (2012)

Analytic model for the efficiency droop in semiconductors with asymmetric carrier-transport properties based on drift-induced reduction of injection efficiency

Appl. Phys. Lett. **100**, 161106 (2012)

Obvious efficiency enhancement of organic light-emitting diodes by parylene-N buffer layer

Appl. Phys. Lett. **100**, 163303 (2012)

Obvious efficiency enhancement of organic light-emitting diodes by parylene-N buffer layer

APL: Org. Electron. Photonics **5**, 93 (2012)

Study of droop phenomena in InGaN-based blue and green light-emitting diodes by temperature-dependent electroluminescence

Appl. Phys. Lett. **100**, 153506 (2012)

Additional information on Appl. Phys. Lett.

Journal Homepage: <http://apl.aip.org/>

Journal Information: http://apl.aip.org/about/about_the_journal

Top downloads: http://apl.aip.org/features/most_downloaded

Information for Authors: <http://apl.aip.org/authors>

ADVERTISEMENT

<p>INSTRUMENTS FOR ADVANCED SCIENCE</p> 		<p>Gas Analysis</p> <p>dynamic measurement of reaction gas streams catalysis and thermal analysis molecular beam studies dissolved species probes fermentation, environmental and ecological studies</p>	<p>Surface Science</p> <p>UHV TPD SIMS end point detection in ion beam etch elemental imaging - surface mapping</p>	<p>Plasma Diagnostics</p> <p>plasma source characterisation etch and deposition process reaction kinetic studies analysis of neutral and radical species</p>	<p>Vacuum Analysis</p> <p>partial pressure measurement and control of process gases reactive sputter process control vacuum diagnostics vacuum coating process monitoring</p>
<p>contact Hiden Analytical for further details: info@hiden.co.uk www.HidenAnalytical.com CLICK TO VIEW OUR PRODUCT CATALOGUE</p>					

Deep-ultraviolet light-emitting device realized via a hole-multiplication process

H. Zhu,^{1,2} C. X. Shan,^{1,a)} B. H. Li,¹ Z. Z. Zhang,¹ B. Yao,¹ and D. Z. Shen¹

¹Key Laboratory of Excited State Processes, Changchun Institute of Optics, Fine Mechanics and Physics, Chinese Academy of Sciences, Changchun 130033, China

²Graduate University of the Chinese Academy of Sciences, Beijing 10049, China

(Received 27 June 2011; accepted 22 August 2011; published online 9 September 2011)

By proper controlling the carrier generation and multiplication processes, an Au/MgO/Mg_{0.52}Zn_{0.48}O/Mg_xZn_{1-x}O/*n*-ZnO structure has been designed and fabricated. In this structure, holes are multiplied via an impact ionization process in the MgO layer and injected into the Mg_{0.52}Zn_{0.48}O layer, and electrons are injected into the Mg_{0.52}Zn_{0.48}O layer from the *n*-ZnO layer through a composition-gradient Mg_xZn_{1-x}O bridging layer. With the injection of electrons and holes, a deep ultraviolet emission at around 276 nm, coming from the Mg_{0.52}Zn_{0.48}O active layer, has been observed. The results reported in this letter may provide a promising route to high performance deep ultraviolet light-emitting devices. © 2011 American Institute of Physics. [doi:10.1063/1.3637575]

Deep-ultraviolet (DUV) (with wavelengths shorter than 300 nm) light-emitting devices (LEDs) have a variety of potential applications, such as air and water purification, food sterilization, medical diagnosis and therapy, etc.^{1,2} With the increasing awareness of health risks caused by contaminated food, air, and water, demands of purification products based on compact and cost-effective semiconductor UV sources are expanding.³ Generally speaking, to realize an efficient semiconductor light-emitter, a *p-n* junction should be constructed. For DUV LEDs, the bandgap of the active semiconductor layer should be larger than 4.1 eV. Although there have been some reports on DUV emission from wide bandgap semiconductors,⁴⁻⁸ intentional doping, especially *p*-type doping, of such wide bandgap semiconductors is still problematic due to the relatively large activation energies of acceptors. For example, the activation energy of Mg acceptors in GaN based semiconductors increases from 170 meV for GaN to about 500 meV for AlN.⁹⁻¹¹ The large acceptor activation energy makes the realization of viable DUV LEDs through the common *p*-type doping route almost impossible.

It is accepted that under the drive of a relatively high electric field, the carriers in a material can gain much kinetic energy. These energetic carriers can generate additional electron-hole pairs by impacting with the atoms in lattice of the host material. The generated carriers will again gain kinetic energy and impact with the lattice and generate more carriers. The above process is the so-called impact ionization process.¹² Considering that efficient generation of holes by doping is almost impossible in wide bandgap semiconductors, holes might alternatively be generated and multiplied by employing the ionization process, then DUV light-emitters may be realized. We show in this paper that wide bandgap semiconductor based DUV light-emitters can indeed be achieved employing the hole-multiplication process, by passing the problematic *p*-type doping method.

An Au/MgO/Mg_{0.52}Zn_{0.48}O/Mg_xZn_{1-x}O/*n*-ZnO structure has been designed and constructed. In this structure, holes are

generated and multiplied in the MgO layer under a relatively high electric field, and the holes drift to the Mg_{0.52}Zn_{0.48}O layer under forward bias. An *n*-ZnO layer was employed as the electron source from which electrons are injected into the Mg_{0.52}Zn_{0.48}O layer. A composition-gradient Mg_xZn_{1-x}O layer whose composition varies from ZnO to Mg_{0.52}Zn_{0.48}O gradually has been employed to bridge the *n*-ZnO and Mg_{0.52}Zn_{0.48}O layer to facilitate the injection of electrons. In this way, electrons in the *n*-ZnO layer can be efficiently injected into the Mg_{0.52}Zn_{0.48}O layer under the drive of forward bias. As a result, holes and electrons are both injected into the Mg_{0.52}Zn_{0.48}O layer and they recombine there. DUV electroluminescence at around 276 nm has been observed from this structure.

The *n*-ZnO film in the Au/MgO/Mg_{0.52}Zn_{0.48}O/Mg_xZn_{1-x}O/*n*-ZnO structure was grown by an atomic layer deposition technique, and the detailed growth conditions has been described elsewhere.^{13,14} The bridging Mg_xZn_{1-x}O layer with *x* changing gradually from 0 to 0.52 was deposited onto the ZnO film in a plasma-assisted molecular-beam epitaxy system. After that, the active Mg_{0.52}Zn_{0.48}O layer was grown onto the bridging layer. The substrate temperature was fixed at 500 °C and the chamber pressure at 2.5×10^{-6} mbar during the growth processes. Finally, an MgO layer was deposited on the active layer by radio-frequency magnetron sputtering. Au and indium contacts were then deposited onto the MgO and ZnO layer by vacuum evaporation. The Mg composition in the MgZnO layer was determined by energy dispersive x-ray spectroscopy. A Bruker-D8 x-ray diffractometer (XRD) was used to evaluate the crystalline properties of the layers. Photoluminescence (PL) spectra of the layers were recorded in a JY Triax 550 spectrometer, employing the 266 nm line of the fourth-harmonic of a Nd:YAG pulse laser as the excitation source. Electroluminescence (EL) spectra of the structure were recorded in a Hitachi F4500 spectrometer with a continuous-current power source.

Figure 1(a) shows a typical XRD pattern of the Mg_{0.52}Zn_{0.48}O/Mg_xZn_{1-x}O/*n*-ZnO structure. Two peaks at 34.46° and 36.61° can be observed. The former can be indexed to the diffraction from the (0002) facet of wurtzite

^{a)} Author to whom correspondence should be addressed. Electronic mail: phycxshan@yahoo.com.cn.

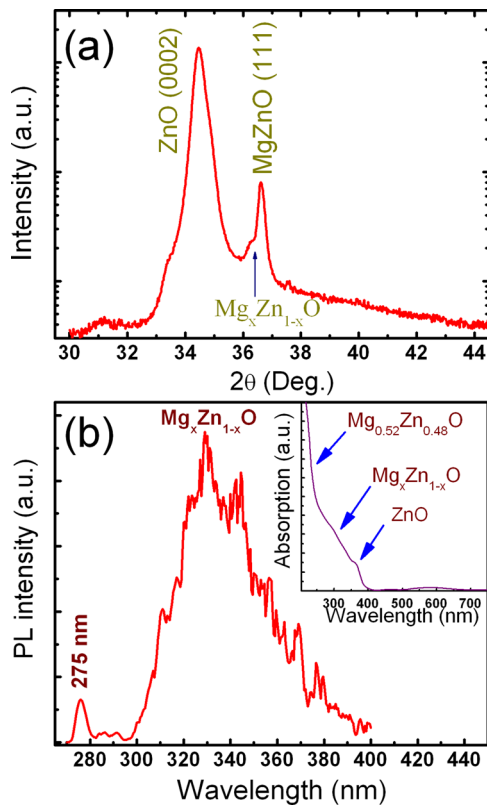


FIG. 1. (Color online) X-ray diffraction pattern (a) and room temperature PL spectrum (b) of the $\text{Mg}_{0.52}\text{Zn}_{0.48}\text{O}/\text{Mg}_x\text{Zn}_{1-x}\text{O}/n\text{-ZnO}$ structure, and the inset of (b) displays its absorption spectrum.

ZnO and the latter to that from the (111) facet of cubic $\text{Mg}_{0.52}\text{Zn}_{0.48}\text{O}$.¹⁵ Noticeably, a shoulder at 36.3° is also visible, which may be identified as diffraction from the $\text{Mg}_x\text{Zn}_{1-x}\text{O}$ layer. The XRD data reveal that the ZnO is hexagonal structured with a c -axis preferred orientation, and the $\text{Mg}_{0.52}\text{Zn}_{0.48}\text{O}$ film has a cubic rocksalt structure.

The room temperature PL spectrum of the $\text{Mg}_{0.52}\text{Zn}_{0.48}\text{O}/\text{Mg}_x\text{Zn}_{1-x}\text{O}/n\text{-ZnO}$ structure is illustrated in Figure 1(b). It displays a DUV emission at about 275 nm, which can be attributed to the near-band-edge (NBE) emission of the $\text{Mg}_{0.52}\text{Zn}_{0.48}\text{O}$ layer.¹⁶ Also a broad emission in the range of 300–370 nm can be observed, which is believed to come from the $\text{Mg}_x\text{Zn}_{1-x}\text{O}$ composition-gradient layer. The inset of Figure 1(b) shows the absorption spectrum of the structure. Two absorption edges at around 380 nm and 270 nm can be observed clearly, and the former comes from the ZnO film and the latter from the $\text{Mg}_{0.52}\text{Zn}_{0.48}\text{O}$ layer. A broad absorption is also visible between the two edges, which is from the $\text{Mg}_x\text{Zn}_{1-x}\text{O}$ composition-gradient layer.

A schematic structure of the DUV device is shown in the inset of Fig. 2. The thickness of the MgO, $\text{Mg}_{0.52}\text{Zn}_{0.48}\text{O}$, $\text{Mg}_x\text{Zn}_{1-x}\text{O}$, and $n\text{-ZnO}$ layer is 60 nm, 400 nm, 100 nm, and 150 nm, respectively. The electron concentration and Hall mobility of the ZnO layer is $2.3 \times 10^{19} \text{ cm}^{-3}$ and $23 \text{ cm}^2/\text{Vs}$, respectively. The Au contact was patterned into an S-shape using photolithography to increase current distribution. Figure 2 shows the current-voltage (I - V) curve of the device. It exhibits an obvious rectification characteristic with a turn-on voltage of about 26.0 V.

The characteristic EL spectra of the device are shown in Figure 3. When the injection current is 30 mA, the spectrum

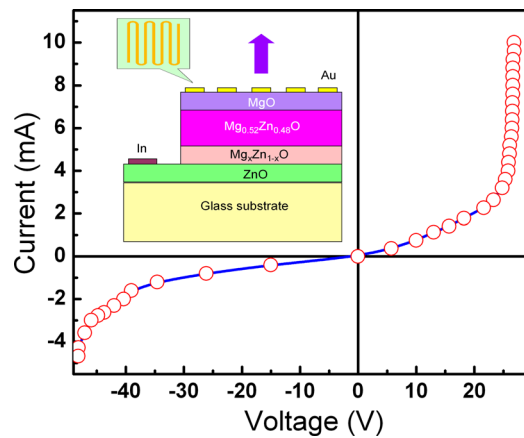


FIG. 2. (Color online) Typical I - V curve of the Au/MgO/ $\text{Mg}_{0.52}\text{Zn}_{0.48}\text{O}/\text{Mg}_x\text{Zn}_{1-x}\text{O}/n\text{-ZnO}$ structure, and the inset shows a schematic illustration of the structure.

shows three weak emission bands at 276 nm, 335 nm, and 500 nm. Because the wavelength of the peak at 276 nm is almost identical to that of the PL peak of the $\text{Mg}_{0.52}\text{Zn}_{0.48}\text{O}$ shown in Figure 1(b) (275 nm), it can be attributed to the NBE emission of the layer. The broad peak at around 335 nm can be attributed to the emission from the $\text{Mg}_x\text{Zn}_{1-x}\text{O}$ layer, for its position is close to that of the PL emission of the layer. The emission at around 500 nm, which has been frequently observed in ZnO-based materials, may come from deep-level emission of the $n\text{-ZnO}$ layer. When the injection current is increased to 40 mA, besides the emissions at 276 nm and 335 nm, a weak tail at around 380 nm appears, which is the typical NBE emission of ZnO. By further increasing the injection current to 50 mA, the NBE emission from the $\text{Mg}_{0.52}\text{Zn}_{0.48}\text{O}$ layer dominates the spectrum, while the emissions from the $\text{Mg}_x\text{Zn}_{1-x}\text{O}$ and ZnO layer are almost undetectable. The inset shows the dependence of output power of the device on the injection current. It can be seen that the output power of the device is in the order of nanowatt and it increases with the injection current.

The mechanism for the DUV emission from the Au/ $\text{MgO}/\text{Mg}_{0.52}\text{Zn}_{0.48}\text{O}/\text{Mg}_x\text{Zn}_{1-x}\text{O}/n\text{-ZnO}$ structure can be understood in terms of the band alignment of the structure

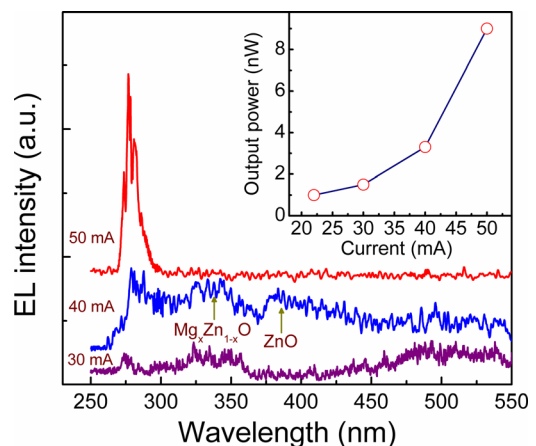


FIG. 3. (Color online) Room temperature EL spectra of the Au/MgO/ $\text{Mg}_{0.52}\text{Zn}_{0.48}\text{O}/\text{Mg}_x\text{Zn}_{1-x}\text{O}/n\text{-ZnO}$ structure under the injection of continuous current, and the inset shows the dependence of output power on the injection current.

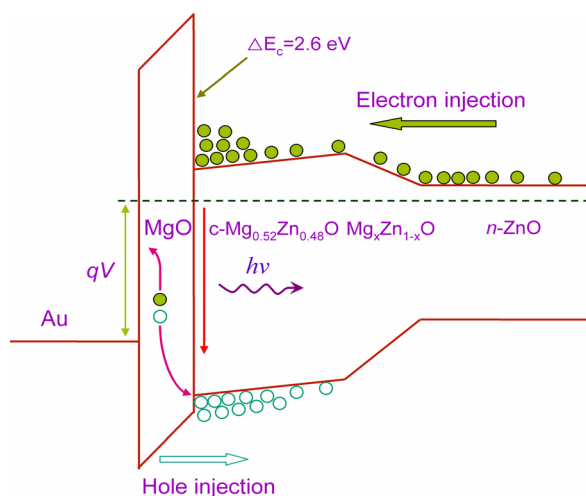


FIG. 4. (Color online) Bandgap diagram of the Au/MgO/Mg_{0.52}Zn_{0.48}O/Mg_xZn_{1-x}O/n-ZnO structure under forward bias showing the generation, multiplication, and injection of electrons and holes.

shown in Fig. 4. Although the *n*-ZnO layer with an electron concentration of $2.3 \times 10^{18} \text{ cm}^{-3}$ can serve as an electron source, the large conduction band offset ($\Delta E_c = 0.9 \text{ eV}$) between it and the Mg_{0.52}Zn_{0.48}O forms a large barrier that hinders the injection of electrons. To solve this problem, a composition-gradient Mg_xZn_{1-x}O layer with *x* changing from 0 to 0.52 gradually has been employed to bridge the Mg_{0.52}Zn_{0.48}O and *n*-ZnO layers to aid the drift of electrons from the latter to the former. Meanwhile, the ΔE_c between MgO and Mg_{0.52}Zn_{0.48}O is as large as 2.6 eV, which forms a large barrier that confines the electrons in the Mg_{0.52}Zn_{0.48}O layer. As a result, electrons will accumulate at the MgO/Mg_{0.52}Zn_{0.48}O interface when driven by a forward bias. Meanwhile, considering that most of the voltage would be applied onto the MgO layer due to its dielectric nature, the electric field in the MgO layer can be in the order of 10^6 V/cm . Under such a high electric field, the carriers in the MgO layer, although few in number, will gain much kinetic energy that leads to impact ionization. The process excites the electrons in the valence band of MgO into its conduction band, leaving free holes. That is, electron-hole pairs can be generated in the MgO layer via the impact ionization process, which has been elucidated in our previous publications.^{17,18} Under a forward bias, the generated holes can inject into the Mg_{0.52}Zn_{0.48}O layer and recombine radiatively with the electrons accumulated at the MgO/Mg_{0.52}Zn_{0.48}O interface. At a low forward bias, few electrons can be injected into the Mg_{0.52}Zn_{0.48}O and Mg_xZn_{1-x}O layers, holes generated in the MgO layer via impact ionization can drift to the Mg_{0.52}Zn_{0.48}O, Mg_xZn_{1-x}O, or even the *n*-ZnO layer, and recombine with electrons in these layers. Therefore, weak emissions from the Mg_{0.52}Zn_{0.48}O, Mg_xZn_{1-x}O and ZnO

layers have been observed, as shown by the 30 mA and 40 mA spectra of the structure shown in Figure 3. While at larger bias, many electrons will be drifted and accumulated at the MgO/Mg_{0.52}Zn_{0.48}O interface, most of the injected holes from the MgO layer will be captured by the accumulated electrons due to the relatively large exciton binding energy of ZnO-based semiconductors. As a result, only emission from the Mg_{0.52}Zn_{0.48}O layer is observed, while those from the Mg_xZn_{1-x}O and ZnO layers are almost undetectable, as indicated by the 50 mA spectrum shown in Figure 3.

In conclusion, a DUV light-emitting device has been fabricated in an Mg_{0.52}Zn_{0.48}O film by properly designing the generation and injection processes of holes and electrons, in which holes are generated and multiplied in the MgO layer via impact ionization, and electrons injected into the Mg_{0.52}Zn_{0.48}O layer from an *n*-ZnO layer through a composition-gradient Mg_xZn_{1-x}O bridging layer. An obvious DUV emission at around 276 nm has been obtained from the structure. The results reported in this letter may provide a promising alternative route to DUV light-emitters.

This work is supported by the National Basic Research Program of China (2011CB302005), the Natural Science Foundation of China (61177040, 11074248, and 10974197), and the Science and Technology Developing Project of Jilin Province (20090124).

- ¹T. Oto, R. G. Banal, K. Kataoka, M. Funato, and Y. Kawakami, *Nature Photon.* **4**, 767 (2010).
- ²K. Watanabe, T. Taniguchi, T. Niiyama, K. Miya, and M. Taniguchi, *Nature Photon.* **3**, 591 (2009).
- ³E. F. Schubert and J. Cho, *Nature Photon.* **4**, 735 (2010).
- ⁴K. Watanabe, T. Taniguchi, and H. Kanda, *Nature Mater.* **3**, 404 (2004).
- ⁵S. Koizumi, K. Watanabe, M. Hasegawa, and H. Kanda, *Science* **292**, 1899 (2001).
- ⁶U. Schwarz, *Nature Photon.* **2**, 521 (2008).
- ⁷M. C. Tsai, S. H. Yen, and Y. K. Kuo, *Appl. Phys. Lett.* **98**, 111114 (2011).
- ⁸H. Hirayama, Y. Tsukada, T. Maeda, and N. Kamata, *Appl. Phys. Exp.* **3**, 031002 (2010).
- ⁹A. Khan, K. Balakrishnan, and T. Katona, *Nature Photon.* **2**, 77 (2008).
- ¹⁰Y. Taniyasu, M. Kasu, and T. Makimoto, *Nature* **441**, 325 (2006).
- ¹¹K. B. Nam, M. L. Nakarmi, J. Li, J. Y. Lin, and H. X. Jiang, *Appl. Phys. Lett.* **83**, 878 (2003).
- ¹²S. M. Sze, *Physics of Semiconductor Devices*, 2nd ed. (Wiley, New York, 1981).
- ¹³C. X. Shan, J. Y. Zhang, B. Yao, D. Z. Shen, X. W. Fan, and K. L. Choy, *J. Vac. Sci. Technol. B* **27**, 1765 (2009).
- ¹⁴S. Y. Pung, K. L. Choy, X. H. Hou, and C. X. Shan, *Nanotechnology* **19**, 435609 (2008).
- ¹⁵S. Choopun, R. D. Vispute, W. Yang, R. P. Sharma, T. Venkatesan, and H. Shen, *Appl. Phys. Lett.* **80**, 1529 (2002).
- ¹⁶J. Chen, W. Z. Shen, N. B. Chen, D. J. Qiu, and H. Z. Wu, *J. Phys.: Condens. Matter* **15**, L475 (2003).
- ¹⁷H. Zhu, C. X. Shan, J. Y. Zhang, B. H. Li, D. X. Zhao, Z. Z. Zhang, B. Yao, D. Z. Shen, X. W. Fan, Z. K. Tang, X. H. Hou, and K. L. Choy, *Adv. Mater.* **22**, 1877 (2010).
- ¹⁸H. Zhu, C. X. Shan, B. H. Li, Z. Z. Zhang, D. Z. Shen, and K. L. Choy, *J. Mater. Chem.* **21**, 2848 (2011).